HEAT TRANSFER WITH VERY HIGH FREE-STREAM TURBULENCE AND HEAT TRANSFER WITH STREAMWISE VORTICES*

Robert J. Moffat, Paul Maciejewski,
John K. Eaton, and Wayne Pauley
Stanford University
Stanford, California

Two experimental programs are reviewed in this report, both related to augmentation of heat transfer by complex flow characteristics. The first program deals with very high turbulence (up to 63%) which has been shown to result in Stanton numbers as much as 5 times the expected values. Results from a large number of trials show that fixing the free stream velocity, x-Reynolds number, turbulence intensity and integral length scale does not fix the Stanton number. Two such cases have been found in which the Stanton number of one was 40% larger than the other. Mean velocity and mean temperature profiles are presented in this report, as well as profiles of turbulence intensity within the boundary layer. Two cases are displayed--one with high heat transfer augmentation (3/1) and the other with low (1.8/1). There are obvious, qualitative differences in the profiles

The second program deals with vortices originating at bluff bodies and traveling downstream embedded in the wall boundary layer. Velocity vector maps from the boundary layers and distributions of Stanton number on the wall are presented for three types of bodies: square, cylindrical, and teardrop.

The heat transfer and velocity maps do not show evidence of the expected "horseshoe vortices" but, instead, show a strong common-flow-up vortex pair. The fluid mechanic mechanism responsible for this secondary flow field has not yet been identified.

Foreword

Most heat transfer research is conducted in low-turbulence tunnels, that is, with less than 0.5% turbulence, in flows especially refined to be spanwise uniform and steady. These conditions produce a "low-limit" estimate of heat transfer for a given mean flow and geometry. Free stream turbulence, or unsteadiness, or streamwise vortices increase heat transfer.

* This work was performed under NASA NAG 3-522.

Free stream turbulence of 4 to 6% or larger may increase heat transfer even in fully turbulent regions [Blair, Ref. 1].

Gas turbines, on the other hand, run with turbulence up to 20-30%, which is probably highly anisotropic and well laced with large coherent structures coming downstream from the combustion chamber. Dils and Follansbee [Ref. 2] measured up to 16% in the discharge of a laboratory scale combustor in a bench test. They reported increases in heat transfer of over 50% on the stagnation line of a cylinder in that flow. Other recent observations (Rohde, [Ref. 3]) suggest 20 to 30% as a reasonable value for the relative turbulence near a typical first turbine nozzle ring.

The flow through a gas turbine may not look much like the flow most researchers have in mind when they think of "turbulence." It is not difficult to imagine, superimposed on the "normal" turbulent fluctuation, a whole family of flow disturbances whose spatial and temporal characteristics are determined by the engine configuration upstream of the point observation.

Among the phenomena which may be present (either intermittently or steadily) are:

(1) large scale, low frequency quasi-coherent structures,
(2) streamwise vortices,
(3) wakes from upstream vanes or blades,
(4) regions of high turbulent shear stress.

This paper describes recent results from two programs at Stanford, one concerning the effects on heat transfer of very high free-stream turbulence and the second concerning the effects of streamwise vortices.

The high turbulence has, so far, been created by placing the test plate in the margin of a large diameter free jet. This exposes the plate to a flow in which the local turbulence intensity can be as high as 70%. Putting the plate at different distances from the jet exit, and at different distances from the axis of the jet allows a certain degree of independence in choosing the mean velocity, turbulence intensity, and the integral length scale.

There is no assurance that this flow is like that which exists in a gas turbine, but it need not be the same to provide clear evidence that chaotic, unsteady, and highly Turbulent (with a capital T!) flows can result in heat transfer rates for higher than predicted by the usual correlations. One objective of this program is to demonstrate how high the "upper bound" of turbulent heat transfer can be pushed, at a given x-Reynolds number based on mean velocity. This will not prove where the upper bound is in a gas turbine, but will show at least where the lower limit of that upper limit might be. A second objective is to identify the turbulence descriptors which best relate to the increased heat transfer. This latter issue is critically important, since we must know what aspect of turbulence

best correlates with the increase in heat transfer before we can specify the measurements which must be made.

It would be very helpful to have a "good" description of the flow field in an engine, to guide the present experiments, but such data are not available. In fact, the present work has already raised some troubling questions about the sufficiency of the usual set of turbulence measures. The issue is, "What aspect of a turbulent flow field best correlates with the increase in heat transfer?" There is no assurance that measures of the mean velocity, turbulence intensity, and integral length scale will suffice to identify the heat transfer aspects of a flow. In fact, the work reported at HOST last year already contained evidence that fixing these three parameters did not fix the heat transfer. Until we know what aspect of the flow to measure, we cannot even enter a sensible request for "Engine Data."

The second program reported here concerns streamwise vortices, and their effect on heat transfer to turbulent boundary layers. This issue has attracted much attention over the last several years, chiefly with regard to the end-wall heat transfer. Several different vortical structures have been identified by flow visualization, but characterization of their effect on heat transfer has been slow in coming. This report describes some of the hydrodynamic features of a streamwise vortex pair which might relate to their effect on heat transfer. These results are described in the section entitled Phase II -- The Effects of the Streamwise Vortices.

Phase I: High Turbulence

This is an experimental program aimed at answering the following questions: (1) How much can free-stream turbulence raise convective heat transfer, all other factors remaining constant? (2) What measurable aspects of the turbulence form the "necessary and sufficient set" needed for predicting the augmentation? (3) How can the effects of turbulence be incorporated into current boundary layer heat transfer models?

Heat transfer experiments are being conducted with highly turbulent air flow over a smooth surface, with free-stream intensities from 15% to 65%. This covers a higher range than is believed to be present in gas turbines, by about a factor of two. These high turbulence levels are generated in the flow field of a large diameter (about 0.3 meter), low velocity (up to 5 meters/sec) free jet discharging into still air. The auto-correlation length scales can be large, up to 17 centimeters, but vary with distance from the nozzle so that different values can be found in the flow and the turbulence intensity varies both radially and axially. Different combinations of free-stream velocity, turbulence intensity, and integral length scale can be found by moving the leading edge of the plate to different locations within the jet. Using the known properties of a free jet and considering the jet initial velocity as a variable, one can plan sequences of trials in which the heat transfer can be measured at pairs of

different locations in the jet which have the same measurable flow properties (i.e., the same mean velocity, turbulence intensity, and integral length scale).

The general arrangement of the hardware is shown in Figure 1. The test surface is an Aluminum plate, 2 meters in length and about 0.5 meter wide, divided into 8 streamwise sections, each a separately instrumented heat transfer specimen. Two orientations are shown for the plate: parallel to the centerline of the jet and parallel to a ray. These result in slightly different distributions of mean velocity along the plate, one case corresponding to a flat plate, the other to a slightly accelerating flow. The free stream velocity and the turbulence intensity both drop off slightly with length along the test plate, but the variations are within +/- 10% of the mid-length values. Those are used to describe the flow. The effect of the radial distribution of velocity in the jet is still measurable near the outer edge of the plate boundary layer.

It was shown, in the 1985 HOST report, that the test plate was "qualified" in that it produced results within +/- 2% of the accepted flat plate correlation, when used in a low turbulence tunnel. It was also shown that the high turbulence flow field of the free jet produced a repeatable heat transfer situation, by a demonstration that two independent "build-ups", i.e., dismounting and re-mounting the plate into the same nominal location in the jet on consecutive days yielded the same data within +/- 2%. On the basis of those tests, it is felt that the results presented here are credible.

The first question, "How much can free-stream turbulence raise convective heat transfer, all other factors remaining constant?", is addressed in Figure 2 which shows that Stanton number augmentation by as much as a factor of 5 has been achieved. Previous work reported in the literature by many sources has shown that turbulence of less than 6% produced only small effects on heat transfer, with occasional reports of "no effect at all". The present results show that turbulence intensities from 20% to 60% can raise the Stanton number by factors of from 1.8 to 5.

The second question, "What measurable aspects of the turbulence form the 'necessary and sufficient set' needed for predicting the augmentation?" is also addressed in Figure 2. Four candidate descriptors are used in constructing this figure: free stream velocity, Re_x, turbulence intensity, and the integral length scale. No combination of these four constitutes a sufficient set, as can be seen by examining the combinations covered in this set of "paired comparison" runs. Numbering the runs from the top down, Runs 1 and 3 contain points at the same X-Reynolds number and turbulence intensity, yet the Stanton number augmentation differs by the ratio of 5 to 3, thus those two descriptors are not sufficient to uniquely define the augmentation. Runs 2 and 5 contain points at the same X-Reynolds number, free-stream velocity, turbulence intensity and integral length scale and yet their augmentation ratios are in the ratio 3 to 2.5 so even the set of four does not uniquely establish the augmentation to better than +/- 13%. Since the experiment has demonstrated repeatability to

within +2% it is evident that +13% is significant. Most current theories in the effects of turbulence describe the response of the boundary layer in terms simply of two (e.g. Reynolds number and turbulence intensity) or three parameters (Reynolds number, turbulence intensity, and length scale). The differences in the present data for the same values of these parameters strongly suggest that these theories cannot be reliable.

The experiments shown in Figure 2 have not yet identified the 'necessary and sufficient set' but have shown that no combination of the four tested are sufficient. No theory can be entirely correct which is based only on those four, since fixing all four does not uniquely determine the augmentation. The problem may be simpler at higher Reynolds numbers, and these four (or even fewer) may be sufficient in that regime but, for the present flow conditions, it seems clear that some additional descriptor must be found.

In the first series of experiments a single U-component hot-wire anemometer was used to estimate the mean velocity, turbulence intensity, integral length scale, even though its limitations were clearly recognized.

A single hot-wire probe cannot accurately describe the details of the free stream turbulence since it is sensitive to more than one component of the flow and yet does not accurately represent the total velocity. To investigate the magnitude of the error involved, an orthogonal triple-wire probe was used to measure the free stream turbulence properties. Its results confirmed the single-wire results within reasonable accuracy and, based on the findings already mentioned, we began to examine the details of the turbulence in two selected cases: High Augmentation and Low Augmentation.

Progress During the Past Year

Experiments during the past year were concentrated on obtaining more detailed turbulence measurements in the free stream and temperature and velocity profiles in the boundary layers. The objective in these profile measurements was to answer the following questions: (1) "How do the velocity and temperature distributions differ between the high augmentation and the low augmentation cases?", and (2) "How do the details of the free stream turbulence differ between the high and low augmentation cases?"

This question was addressed by using an orthogonal triple-hot-wire in the free stream, with analog processing capable of time-resolved measurements of the individual components of the Reynolds stress tensor and by two traversable probes for the boundary layer, a single-wire constant temperature anemometer for mean and fluctuating velocity measurements and a fine-wire thermocouple probe for mean temperature.

Within the boundary layers, the distributions of velocity and temperature were compared for the two cases -- high augmentation and low. The Stanton number data for the two cases are shown in Figure 3. These will be referred to in the following figures as the High Augmentation and the Low Augmentation cases not by their turbulence measure. Note that even in the "Low Augmentation" case, the Stanton number is higher than the usual flat plate value by a factor of 1.8, while the High case is up by a factor of 3.

Figure 4 presents the mean velocity distributions for both cases in $u^+ - y^+$ coordinates, at three locations along the test plate. The value of $C_f/2$ was assumed equal to the Stanton number. Experiments supporting this assumption were done last year. It was shown in those experiments that the turbulent shear stresses measured in the boundary layer using the triple-wire probe, if extrapolated to the wall, were in reasonable agreement with that assumption.

In one respect these data resemble rough-wall results: the log region is depressed proportionately more in the high augmentation (high turbulence) case than in the low. In addition, however, the log region for the high augmentation case displays a lower slope than the low augmentation case; evidently the mixing process in the boundary layer is significantly different in the two cases. There is no evidence of a wake region in either set of profiles.

These data appear somewhat irregular in the outer region, and one might wonder why. In fact, it is a non-trivial task to acquire representative data in the outer region of the boundary layer in this flow field -- there are some very long-period excursions in the flow. Figure 5 compares mean velocity profiles taken by two traversing strategies: 1000 measurements at each station, serially measured from the wall out to the free stream ("munching") and 30 measurements at each station, on each of 30 traverses, with the data then averaged ("looping"). The total time span of each acquisition was approximately 2.5 hours. Note that the "looping" strategy randomized the long period excursion of velocity which introduced the pathology in the "munching" profile. This long period excursion is believed to be due to meandering of the jet centerline, a large scale phenomenon which, if it is in fact present, would be scaled partly on the room dimensions, not only those of the jet. The turbulence profiles are less affected by the choice of traversing strategy since slow variations in the mean are not recorded. All of the data presented here were acquired by "looping" through the boundary layer and averaging the data sets.

Figure 6 compares the turbulence intensities deduced from the single-wire probe for the High and Low augmentation situations. In the High augmentation case, the turbulence intensity distribution resembles the mean velocity distribution itself, at least in its principal features. There appears to be a nearly-log region, and an inner region. Turbulence intensity is high throughout the inner region of the boundary layer, and there is no local "bulge" in the region usually associated with turbulence production in a normal boundary layer. The Low augmentation case does

show some evidence of a local increase, around y^+ of 20 to 30, but there is no pronounced bulge in that data either. In both situations the distributions of turbulence intensity are more like profiles of a conserved property than like the usual turbulence distributions.

Figure 7 shows that the mean temperature distributions at different x-locations are similar within each data set, (High and Low augmentation), but that the two flow fields produce different average profiles. There is one exception to this: the profile from the first segment of the low augmentation situation resembles more the high augmentation data than the low.

The RMS temperature fluctuations were measured for both cases and significantly higher values were found in the high augmentation case. The data are not shown, since no way could be found to deduce the level of fluctuations in the gas temperature from the recorded fluctuations in thermocouple temperature. With high turbulence and simultaneous velocity and temperature fluctuations, the usual time-constant compensation techniques cannot be justified.

Measurements in Highly Turbulent Flows

The work planned for this year involved a more detailed examination of the turbulence properties of the High and Low augmentation situations. In particular, we sought to measure the spectra and energy contents of each of several individual components of the Reynolds stress tensor. This requires accurate measurement of the individual components, which required a careful examination of the triple-wire response to high turbulence.

In the free stream, where turbulence intensities approach 65%, even the real-time-processes orthogonal-triple-wire data are subject to errors due to the instantaneous velocity vectors lying outside the measurable cone. Even if these errors only slightly affected the measurement of total turbulence intensity, they could seriously distort the measurements of the individual Reynolds stress tensor components. Thus, before detailed measurements in the high turbulence free-stream could be trusted, some means was needed for estimating the errors which might be present--in terms of the indicated data. The data acquisition was halted and attention turned to NRI development of a theory and method for estimating the errors. The results of this study are presented as a separate topic, in the next section of this report, but Figure 8, 9, and 10 show one way in which these errors affect the distribution of measured instantaneous velocities.

Figure 8 shows a histogram of 15,000 measurements from a single-wire probe in the free-stream flow of the Low Augmentation case where the turbulence intensity was about 17%. The dotted line represents the measurements while the dashed line is a normal distribution corresponding to the mean and variance of the set of 15,000 points. The agreement is

good, except very near the tails of the distribution. The turbulence is low enough, compared to the mean velocity, that the instantaneous effective velocity (for the hot wire) is dominated by the u-component. The fact that the observed distribution closely resembles the expected (normal) distribution also confirms that the flow field is a normally developing free jet flow.

The High Augmentation case is shown in Figure 9. The dotted line again shows a histogram of 15,000 measurements from a single-wire probe in the free stream flow. The dashed line is the normal distribution associated with the measured data, using Figure 11 (in the next section) as a guide to estimating the true mean and true intensity. Use of Figure 11 for a single-wire is an approximation since Figure 11 was derived for an orthogonal triple-wire. The pathology in the histogram (in the low and negative velocity region) reflects two mechanisms: (1) the probe cannot accurately measure velocity components which lie too close to the wire and, (2) the probe rectifies negative velocity components (those which approach from downstream) and "reports" them as positive. As a consequence, the hot-wire probe "folds" the velocity data across a value near zero, and puts spurious data into the low velocity part of the histogram.

To check that the interpretation proposed for the data in Figure 9 was correct, a computer experiment was performed to simulate the behavior of a triple wire. An artificial data set was generated consisting of 1024 individual realizations (u,v,w) calculated assuming an isotropic, joint-normal probability distribution for a specified mean velocity and turbulence intensity. Each triad was then processed through the response equations of the orthogonal triple-wire, assuming real-time data processing, as is used on the Stanford triple-wire system to eliminate the time-averaging ambiguity. The results of these calculations were then interpreted through the triple-wire velocity decomposition algorithm to yield 1024 values of the apparent u-component. These were then used to generate the histogram shown as the dotted line in Figure 10. This dotted line represents the histogram which would have been deduced from the triple wire if it had been in the hypothetical flow. The dashed line is the normal distribution associated with the hypothetical data set--the real u-components of the simulation set. All of the features of Figure 9 (from a single wire) are consistent with the present simulation of the triple-wire behavior. Figure 10 was generated assuming "critical reflection" at the wire angles, with accurate measurements everywhere within the cone and (except for sign) outside. There may not be a need for any more detailed response equations. The present predictions seem adequately accurate, at least for describing the u-component histogram.

The next section presents the theory of the proposed method for deducing the correct values of turbulence properties in a homogeneous, isotropic flow field from the output of an orthogonal, real-time hot wire system.

Estimating the Errors

An orthogonal triple-wire probe can provide accurate measurements of the mean velocities and the turbulence intensities up to levels of about 30% (Ref. 4). At higher turbulence levels, the probes will tend to overestimate the mean velocity and underestimate the turbulence intensity. Even at 30%, there is no assurance that the individual components of the Reynolds stress tensor are correctly measured.

Accurate measurement of the structure of high turbulence flows is becoming increasingly important. The objective of this portion of our research was to investigate means for extending the turbulence range of the orthogonal triple wire to include flows with up to 60% turbulence. The first goal was to demonstrate accurate measurements in a high turbulence, isotropic flow: the free flow of the present apparatus. This would permit accurate characterization of the individual components of turbulence and, possibly, lead to identifying which aspect of the turbulence most nearly correlated with the heat transfer augmentation.

Directional Ambiguity in Triple Wire Anemometry

The triple wire system involves the solution of the following set of equations:

$$\begin{matrix} X^2 \\ Y^2 \\ Z^2 \end{matrix} = [K]^{-1} \begin{matrix} U^2eff1 \\ U^2eff2 \\ U^2eff3 \end{matrix}$$

Because this system of equations involves the squares of the component velocities (X,Y, and Z in a coordinate system formed by the wires), it is impossible to distinguish a positive component velocity from a negative one. The common practice is to assume the instantaneous velocity vector falls in the first octant in X,Y,Z space even though there is a velocity vector in each of the other seven octants that could have produced the same combination of effective velocities on the three wires. This assumption is relatively safe as long as the turbulence is not more than moderately high (up to 30%) and where the probe axis is aligned with the mean flow direction. For higher levels of turbulence, or gross misalignment of the probe with the mean flow direction, the assumption that the instantaneous velocity vector falls inside the first octant fails. In these situations the actual instantaneous velocity vector cannot in general be determined unambiguously from the measured effective velocities.

The Nature of the Errors

To investigate these errors, a computer code was written to generate simulated velocity vector data for isotropic turbulence. The data are random samples from a tri-variate normal population with the three components having the same standard deviation specified as a fraction of the mean vector. These instantaneous velocity vectors were then "measured" using the equations of a triple wire aligned with the mean flow direction. The hot wire signal was calculated using the Jorgensen decomposition. With these equations the same effective velocity was assigned to all eight of the vector locations (quadrants 1-8) the "apparent" velocity (i.e. the velocity which would have been deduced from the hot wire output) was then calculated by mapping vectors falling in octants two through eight in X,Y,Z space into octant one. Figure 11 illustrates the relationship between the statistics of the simulated flow and those that would have been derived from the output of the triple wire. For small to moderately high levels of fluctuations relative to the mean, nearly all the velocity vectors do fall in the first octant and the agreement between the actual flow field statistics and the statistics of the triple wire output is excellent. For levels of turbulence greater than 30% the triple wire systematically overpredicts the mean and underpredicts the turbulence intensity.

Figure 11 can be used directly to correct the data taken with the triple wire in isotropic and nearly isotropic flows such as the free stream used in this study.

Figures 12 through 14 illustrate how Figure 11 was generated, showing the simulated triple wire data in the u-v plane. Each figure is a plot of 1024 data points generated from an isotropic tri-variate normal distribution. Figure 12 appears to contain fewer points than Figures 13 and 14, but that is only because the points are densely nested near the mean. For 20% turbulence substantially all the velocities do lie within the first octant of the triple wire system and the triple wire output is an accurate measure of the flow field. At 40% turbulence some of the vectors are folded into the first octant, as evidenced by the sharp boundary beginning to form at 45 degrees from the mean flow direction (this corresponds to the 54.7 degree orthogonal triple wire cone angle projected onto the u-v plane). For 60% turbulence, the data is even more distorted, demonstrating the shift the mean to a higher value and the reduction of the standard deviation, as seen in Figure 11.

For an arbitrary Reynolds' stress tensor with the probe misaligned with the mean flow direction the errors one will incur using a triple wire in a highly turbulent flow will be somewhat more complicated, but the trends in the errors are expected to be easy to recognize.

Improving the Accuracy

Figures 11 through 14 show that the triple wire system significantly distorts a cluster of velocity data for turbulence levels greater than 30%. The issue now becomes one of identifying the true population from the distorted cluster of data which was gathered. Figure 10 compares the u-component pdf calculated from the triple wire simulation in Figure 14 to the u-component distribution used in the simulation. Although the pdf is significantly distorted on the left-hand side, there is a region on the right-hand side that is not contaminated by the triple wire's mismapping of the flow field. This fact forms the basis for the present theory for dealing with high turbulence data from a triple wire.

The problem of using a triple in highly turbulent flows for the purpose of making mean velocity and Reynolds' stress measurements can be reduced to the problem of determining the actual probabilistic distribution of states of the velocity vector in complete X,Y,Z space given that all real vectors are mapped into the first octant by the measuring process. The triple wire data provides the distribution of states corresponding to the final states when the actual distribution of states is folded into itself to a degree set by the level of the turbulence measured and the degree to which the probe is misaligned from the mean flow direction. A method has been developed for inferring the actual velocity joint pdf from the "folded" data taken with a conventional triple wire, and is discussed next.

Figure 15 represents a bivariate normal joint pdf of u and v. Imagine an angle two theta such that the points falling outside two theta will be folded into the region inside two theta. The result of this folding will be another joint pdf of u and v which is uniquely related to the original joint pdf of u and v. This is the joint pdf of u and v seen through the triple wire. The next step is to construct a two dimensional histogram of triple wire data in the u-v plane. This histogram will contain a region into which little folding of data has occurred as well as a region including significant numbers of folded data points. If the joint pdf of u and v of the actual flow field were bivariate normal, level curves (equal probability lines) in the not-folded-into region of the histogram generated will be elliptical. If even one uncontaminated equal-probability ellipse can be identified, the actual joint pdf of u and v can be inferred.

Several alternative methods have been identified by which one might identify the "undisturbed pdf" given the "folded pdf". The choice of approach depends on the relative extent of the interference region.

The present proposal is to sample u,v,w triads and construct a high-density three dimensional histogram as an estimate of the u,v,w joint pdf seen through the triple wire. The equal-probability lines of this histogram will then be curve-fit to identify their shape and the u,v,w joint pdf of the actual flow. The present approach can, in principle, also be used in shear flows. It is not restricted to isotropic flows.

Verifying the Technique

We are currently developing the software and data acquisition strategy to implement the technique described above for using the triple wire in highly turbulent flow fields. The steps we propose to follow are: (1) simulate data acquisition from the triple wire probe by a computer experiment and determine whether or not the method is practical from a computational point of view, (2) transfer data acquisition to the actual triple wire to see if it demonstrates the same trends as the simulation, and (3) qualify quantitative measurements using the technique in the Stanford 2-D channel reference flow. The 2-D channel is a known flow field that can be accurately measured with the triple wire with the probe axis aligned with the axis of the channel (mean flow direction). Once the actual flow field has been measured and documented we can purposely misalign the probe in the flow field enough to cause any desired fraction of the instantaneous velocity vectors to fall outside the cone delimiting the first octant in X,Y,Z space. The data falling outside the cone will be folded into the cone. The joint pdf measured with the misaligned triple wire probe can then be compared directly to the known joint pdf for the flow in the channel.

If this technique for interpreting the triple wire output can predict the statistics of the flow in the 2-D channel we will then claim that the technique is ready for use with the triple wire to measure mean velocities and Reynolds stresses in highly turbulent flows.

Program for Next Year

The central problem still remains: "What measurable property of the turbulence predicts the augmentation of heat transfer?" The experiments conducted to date have shown that the four most likely candidates (U_∞, T_u, Re_x and λ) do not uniquely determine the augmentation. Proof that this set is not unique has been made by finding two locations in the flow where each of these four have the same value, and yet the heat transfer behavior is different. It follows that no function of these four can be adequate, however complex the form. What remains?

We plan to examine the spectrum and intensity of the individual components of the Reynolds stress test, in particular those dealing with velocity components normal to the wall.

The objective is to find some measurable attribute of the flow with which to complete the "necessary and sufficient" set. The missing attribute may be related to intensity or scale.

A small modelling effort will begin, using a 2-D time-averaged code (Stan6) with a mixing-length closure. The intent is to find out whether or

not the turbulent Prandtl number model recommended for low turbulence flows is valid at high turbulence. This can be done heuristically, by hypothesizing mixing length distributions, matching the experimental velocity profiles and then comparing predicted and measured temperature profiles.

Phase II: Streamwise Vortices

Our research program on embedded vortices has provided detailed data describing the perturbations in both the heat transfer and fluid mechanics behavior caused by various single vortices, vortex pairs, and vortex arrays. Most of the fundamental mechanisms responsible for heat transfer perturbations are now well understood as described in our two recent papers, Eibeck and Eaton, 1986, and Pauley and Eaton, 1987, (Ref. 5 and 6). The remaining question is: What type of embedded vortices are present in realistic flow geometries?

There has been a large amount of recent research examining the detailed heat transfer behavior in the vicinity of obstacles protruding through a boundary layer. These obstacles may represent either a turbine blade or an internal strut in an engine. The vortex wake trailing behind such obstacles has not been examined. The present facility was used to study the downstream perturbation in the boundary layer caused by various shapes of obstacles including circular, square, and teardrop shaped cross sections. The obstacles were installed in the two-dimensional boundary layer wind tunnel used for all of the previous embedded vortex work. The width of each obstacle was approximately equal to the boundary layer thickness and the height spanned the short dimension of the test section. Three-component mean velocity maps and the spatially resolved heat transfer coefficient were measured downstream of each type of obstacle.

The results were very surprising in view of previous assumptions about the vortex flow behind obstacles. Figure 16 shows the secondary flow in the wake behind a cylinder. A large common-flow-up vortex pair is evident in the mean flow. The diameter of the vortex is considerably larger than the boundary layer thickness, approximately 2 cm. A horseshoe vortex would appear as a common-flow-down vortex pair and would be embedded in the boundary layer. Clearly the present measurements are showing a different phenomenon. Figure 17 shows the heat transfer data behind the same circular cylinder. There is a very large perturbation in the heat transfer rate which can be explained in terms of the observed common-flow-up vortex pair.

Figure 18 provides a comparison between the secondary velocity plots for the wakes behind the three different shapes of obstacles. All three show a large common-flow-up pair but there are considerable differences in the details. There is no evidence of the classical horseshoe vortex in any of these flows. Heat transfer profiles at one axial station

(Figure 19) show that the square and cylindrical obstacles cause similar heat transfer perturbations. The teardrop shape causes a considerably weaker perturbation in general agreement with lower measured secondary flows.

The explanation for this unexpected behavior is not clear at this time. We believe that it has to do with the behavior of a Karman vortex street at an endwall. The vertical axis vorticity in the vortex street is rotated by the boundary layer shear at the endwall and results in longitudinal vortices. We cannot explain why this effect has not been observed previously. The parameters selected for the present experiment, in particular the ratio of the cylinder diameter to the boundary layer thickness may have a strong effect on the downstream flow.

References

1. Blair, M. F., "Influence of Free-Stream Turbulence on Turbulent Boundary Layer Heat Transfer and Mean Profile Development. Part I: Experimental Data," Journal of Heat Transfer, 105:33-41, February 1983.

2. Dills, R. R., and Follansbee, P. S., "Heat Transfer Coefficiency around Cylinders in Crossflow in Combustor Exhaust Gases," Jn. Eng. for Power, October 1977.

3. Rohde, J., "Personal Communication," 1984.

4. Frota, M. M., "Analysis of the Uncertainties in Velocity Measurements and Techniques for Turbulence Measurements in Complex Heated Flows with Multiple Hot Wires," Stanford University PhD Dissertation, Department of Mechanical Engineering, August 1982.

5. Eibeck, P.A. and Eaton, J.K. (1986) "The effects of longitudinal vortices embedded in a turbulent boundary layer of momentum and thermal transport," Proceedings of the Eighth Int'l Heat Transfer Conf., San Francisco, pp. 1115-1120.

6. Pauley, W.R. and Eaton, J.K. (1987) "The Effect of Embedded Longitudinal Vortex Pairs on Turbulent Boundary Layer Heat Transfer," to be presented at 2nd Int'l Symposium on Transport Phenomena in Turbulent Flows, Tokyo.

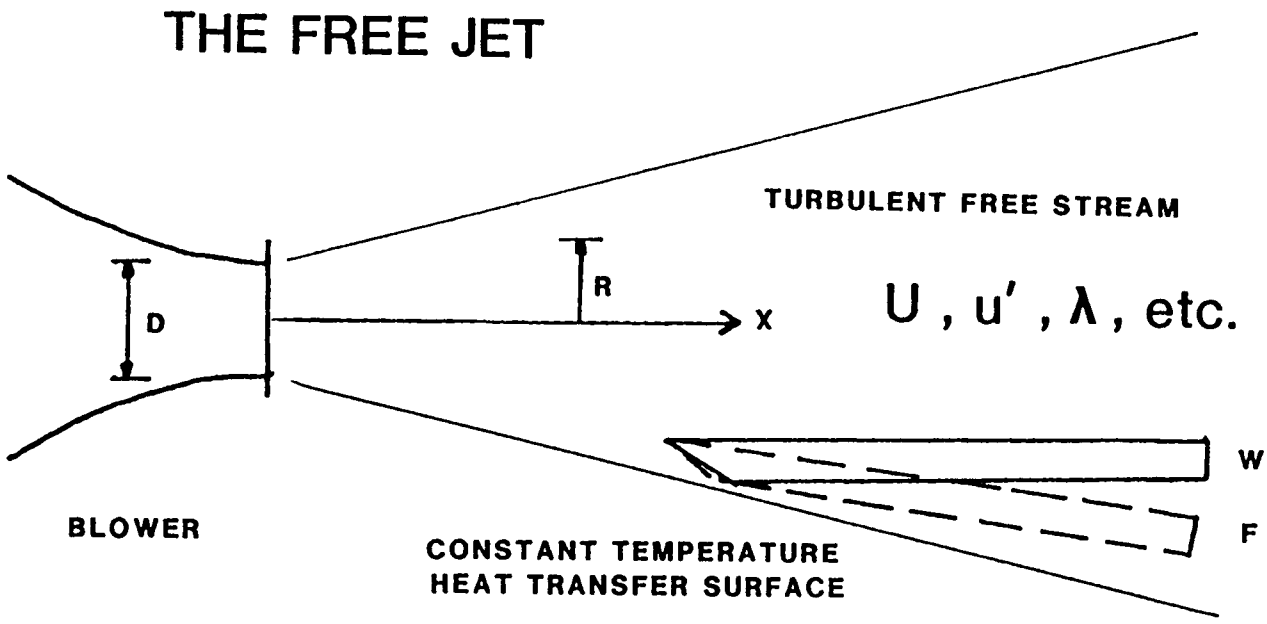

Figure 1 Schematic of the experiment on the effects of high turbulence on heat transfer.

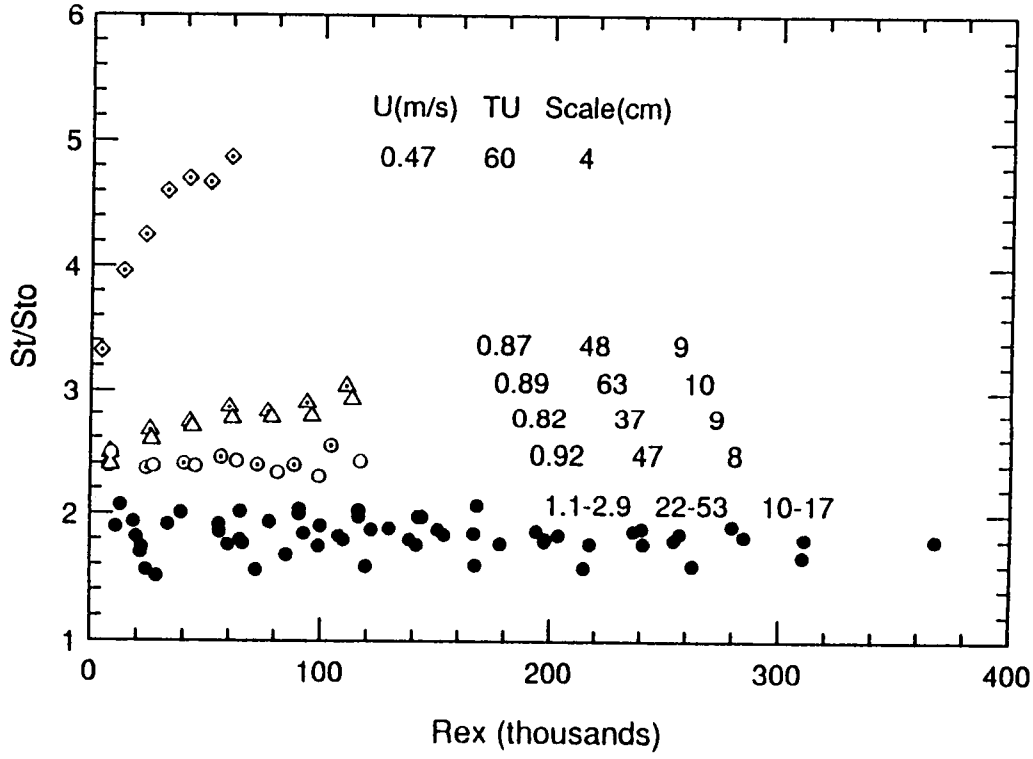

Figure 2 Comparison of hydrodynamic conditions associated with augmented heat transfer.

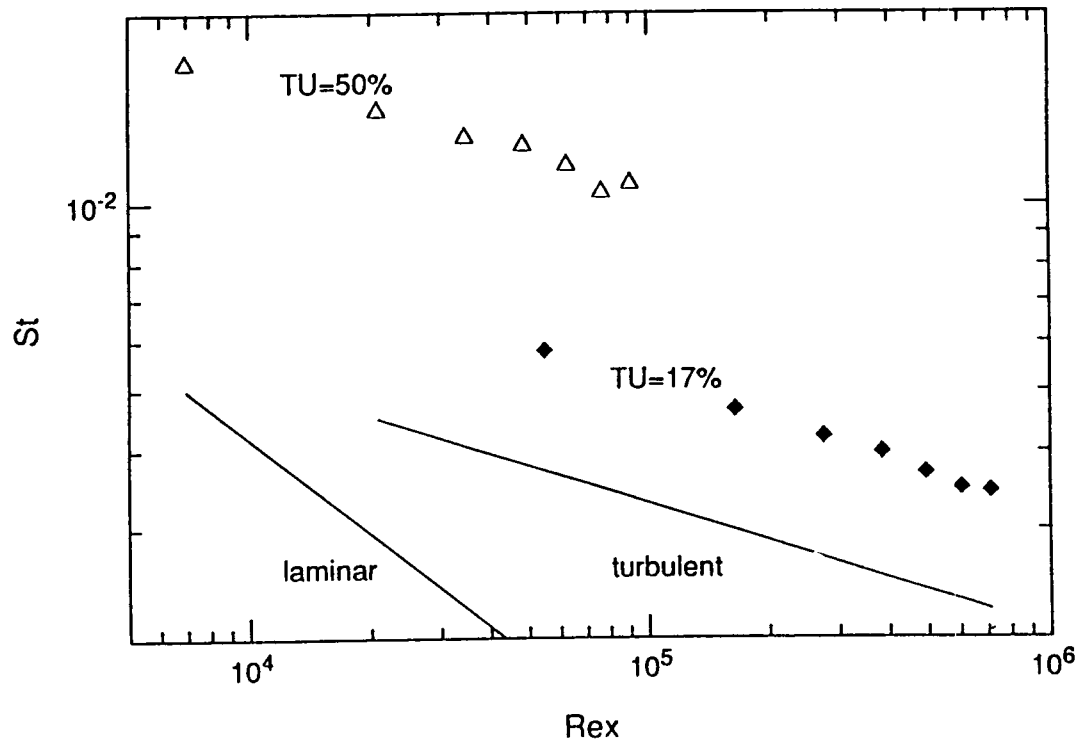

Figure 3 Heat transfer associated with data presented in Figures 4 through 9.

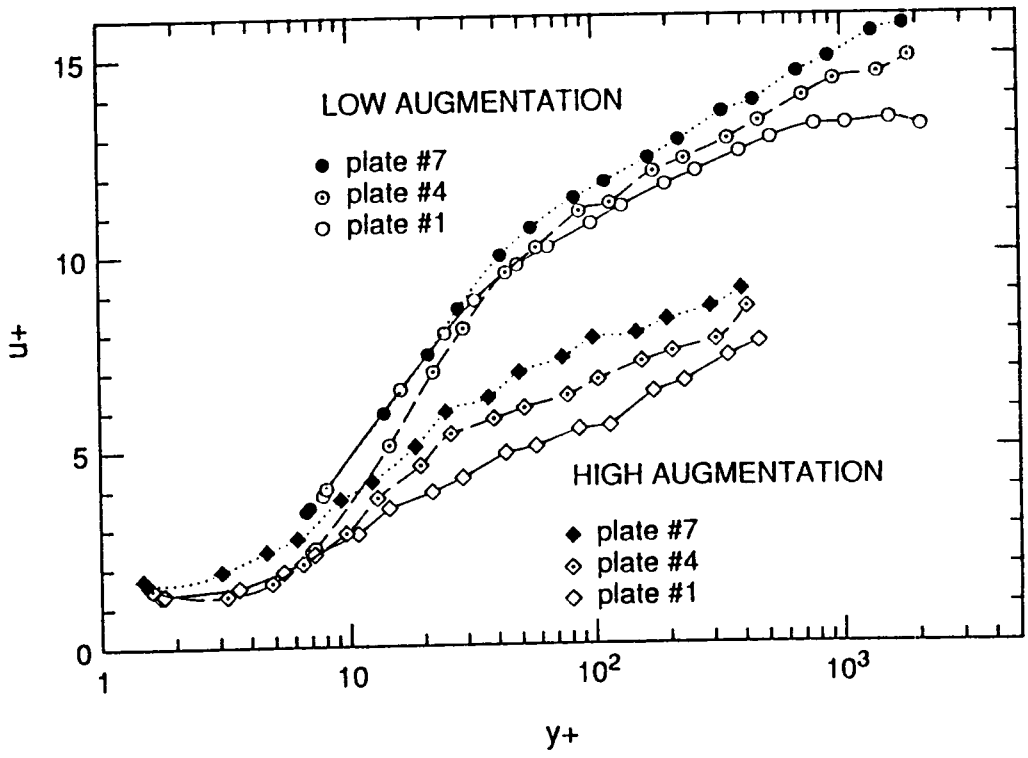

Figure 4 Mean velocity profiles.

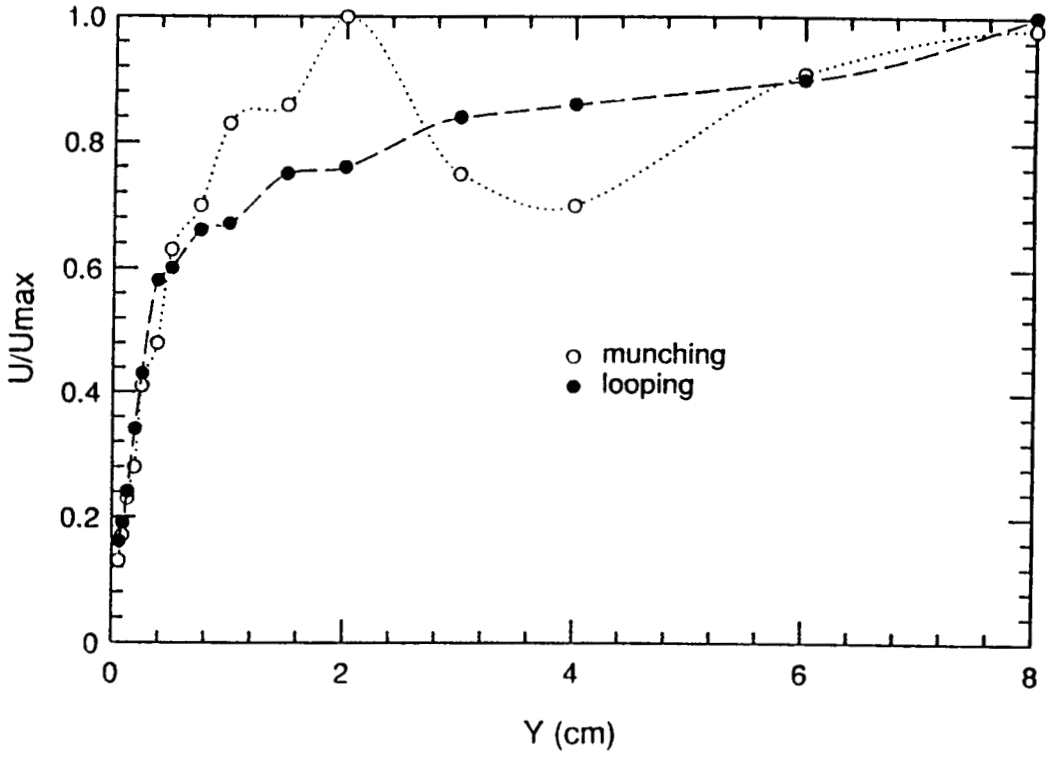

Figure 5 Velocity profiles using two traversing strategies.

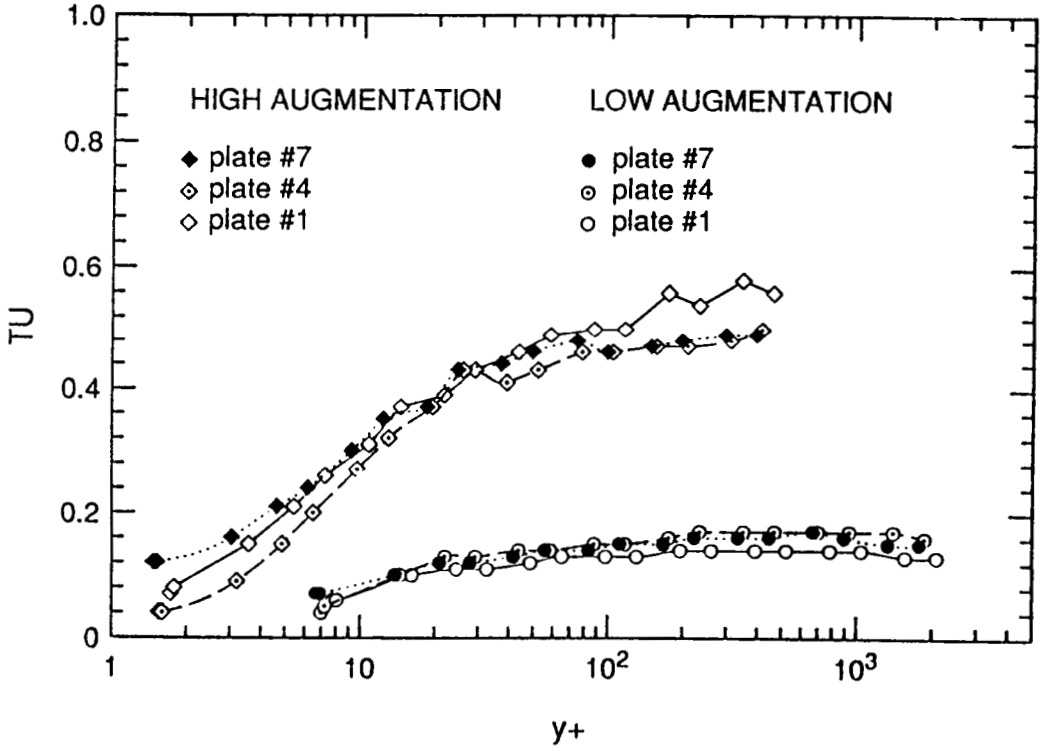

Figure 6 Turbulence intensity profiles.

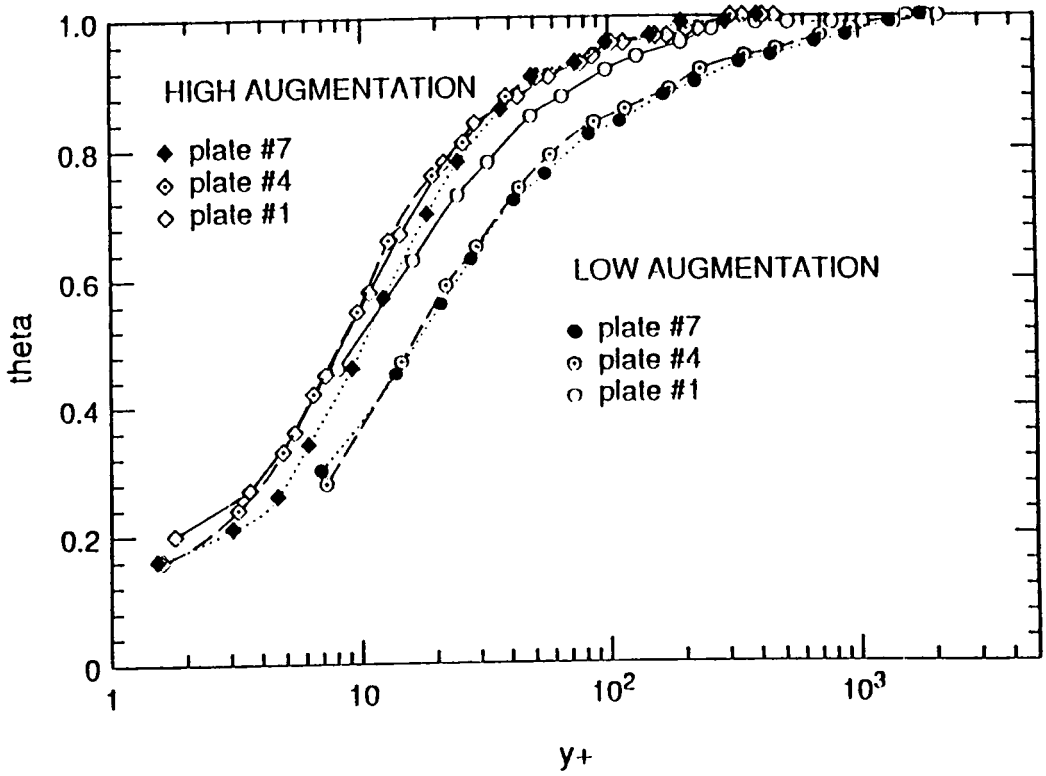

Figure 7 Mean temperature profiles.

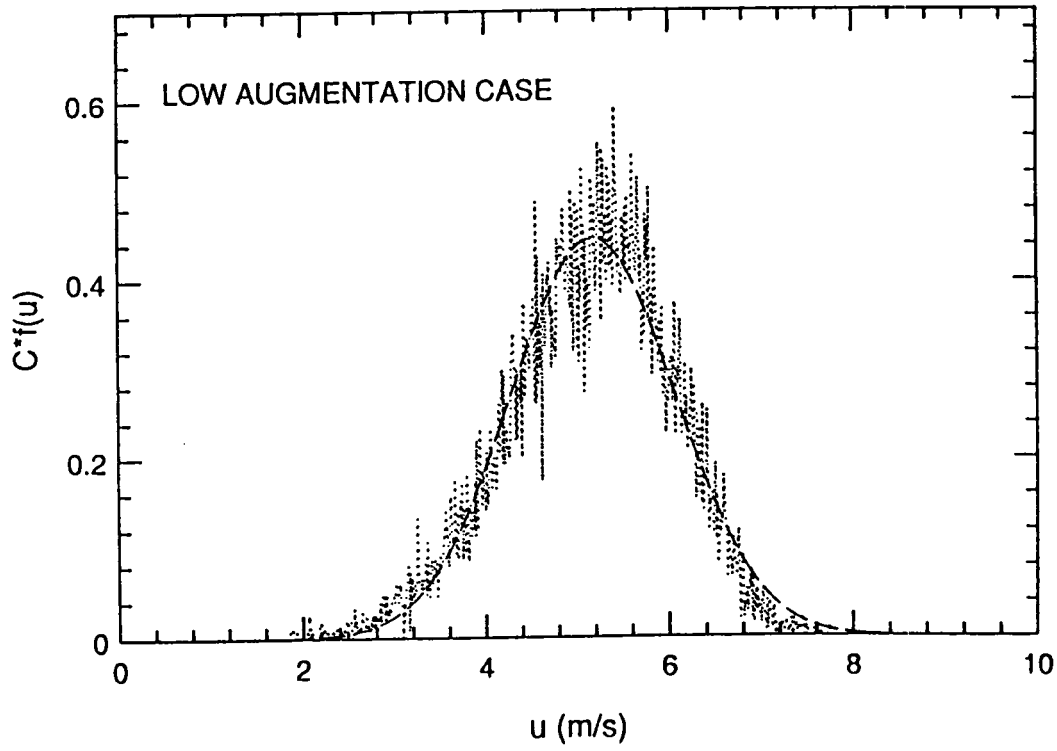

Figure 8 Free stream velocity pdf for low augmentation case.

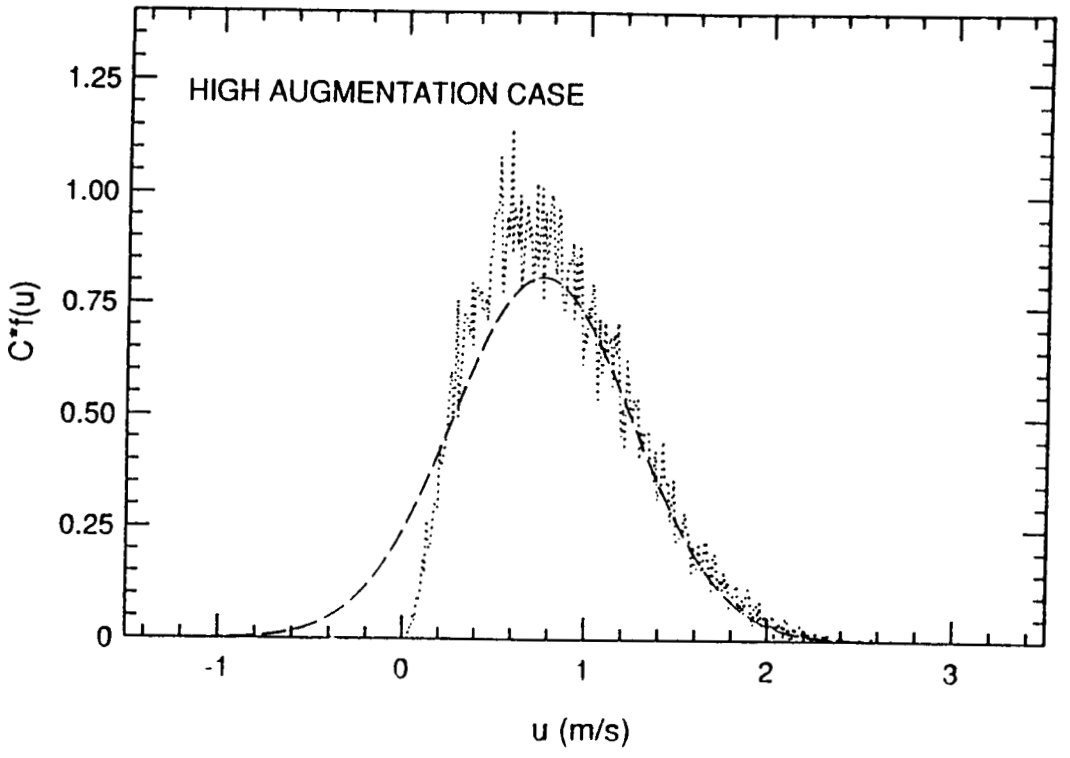

Figure 9 Free stream velocity pdf for high augmentation case.

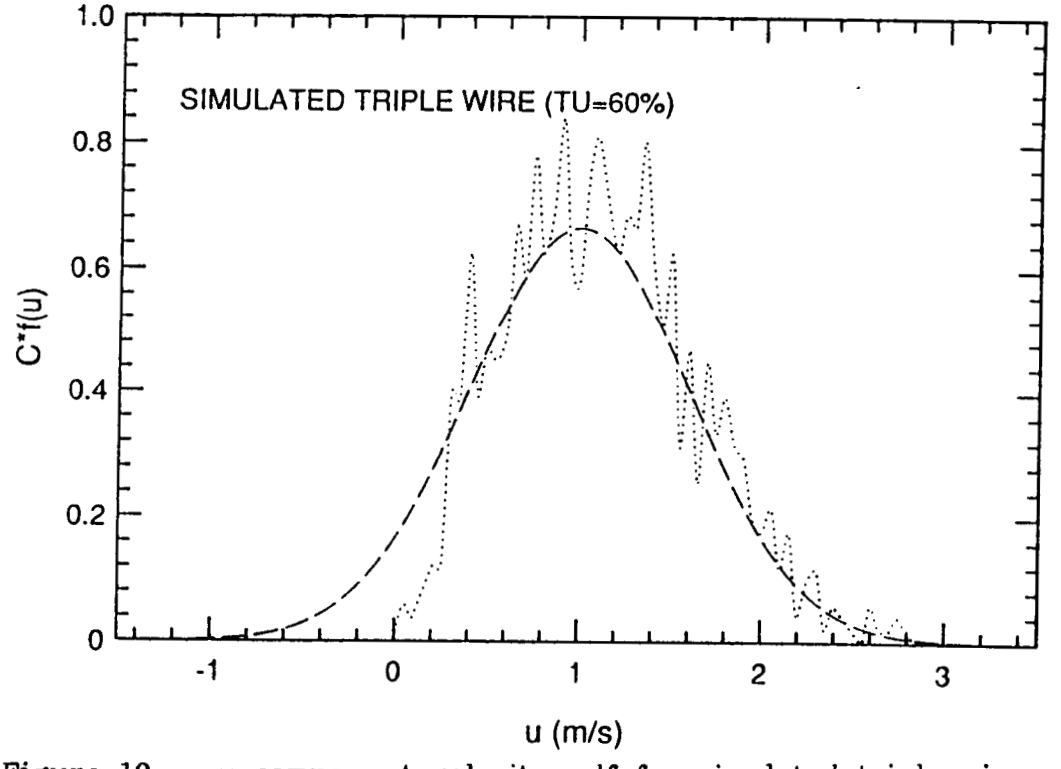

Figure 10 u-component velocity pdf for simulated triple wire.

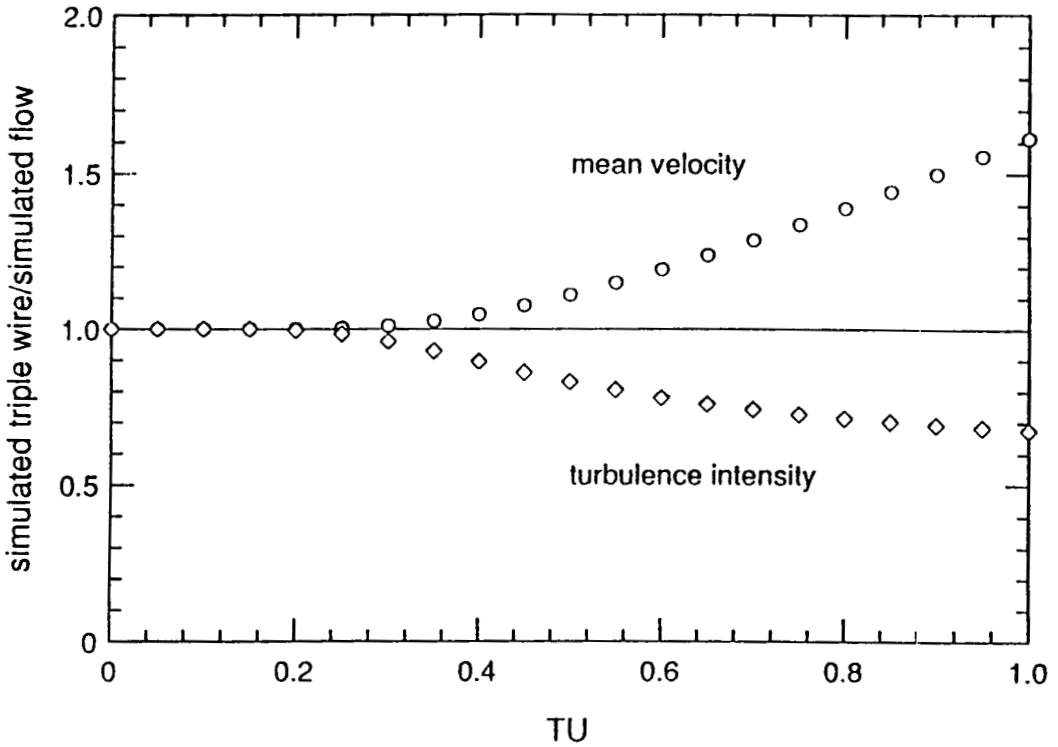

Figure 11 Effects of high turbulence on triple wire output.

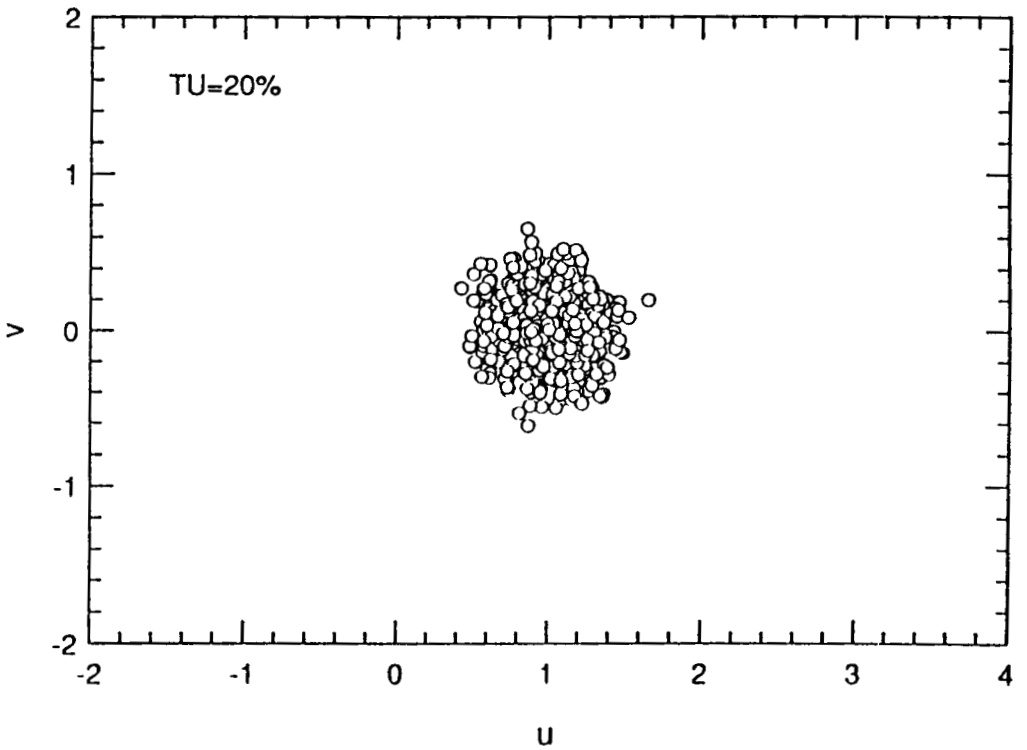

Figure 12 Simulated triple wire data in the u-v plane ror 20% isotropic turbulence.

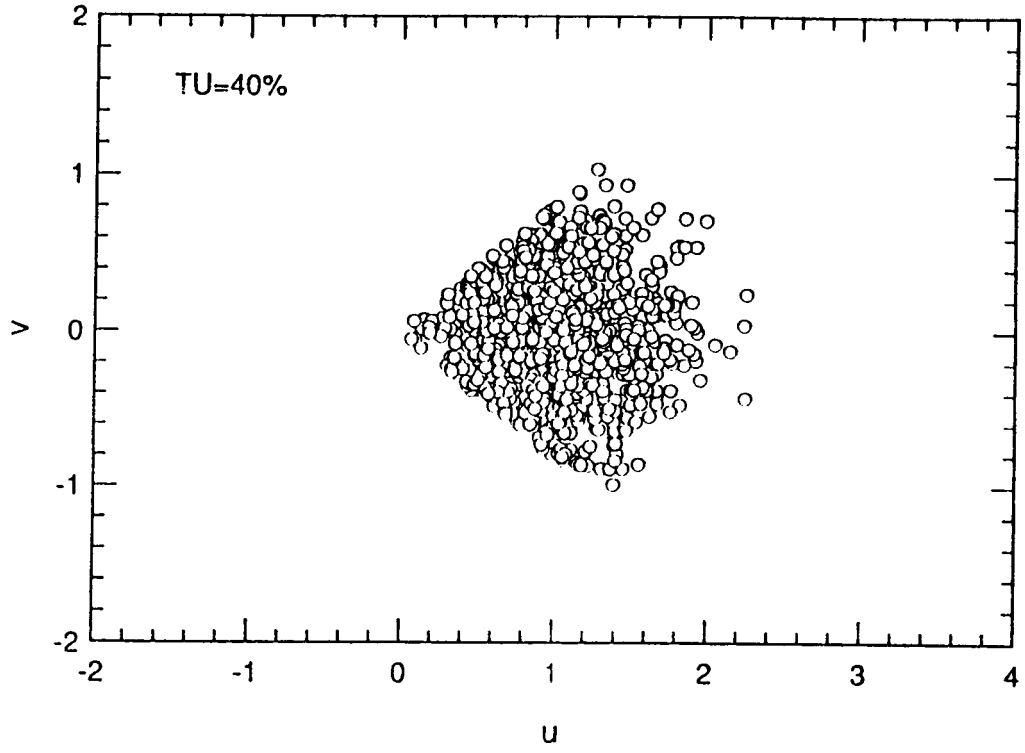

Figure 13 Simulated triple wire data in the u-v plane for 40% isotropic turbulence.

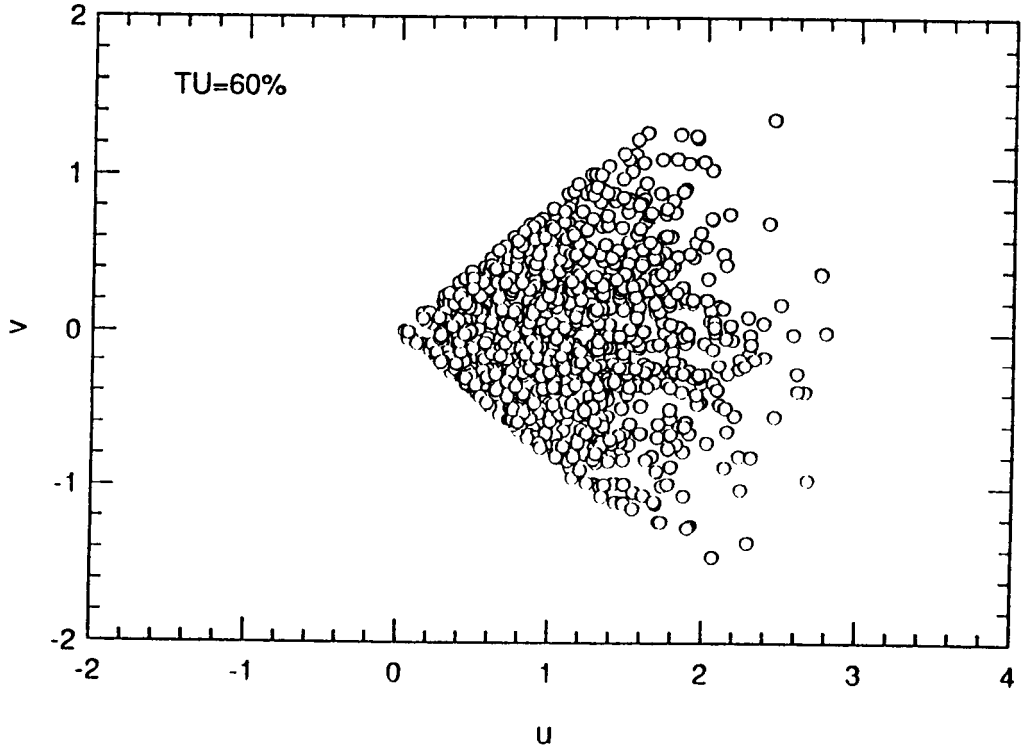

Figure 14 Simulated triple wire data in the u-v plane for 60% isotropic turbulence.

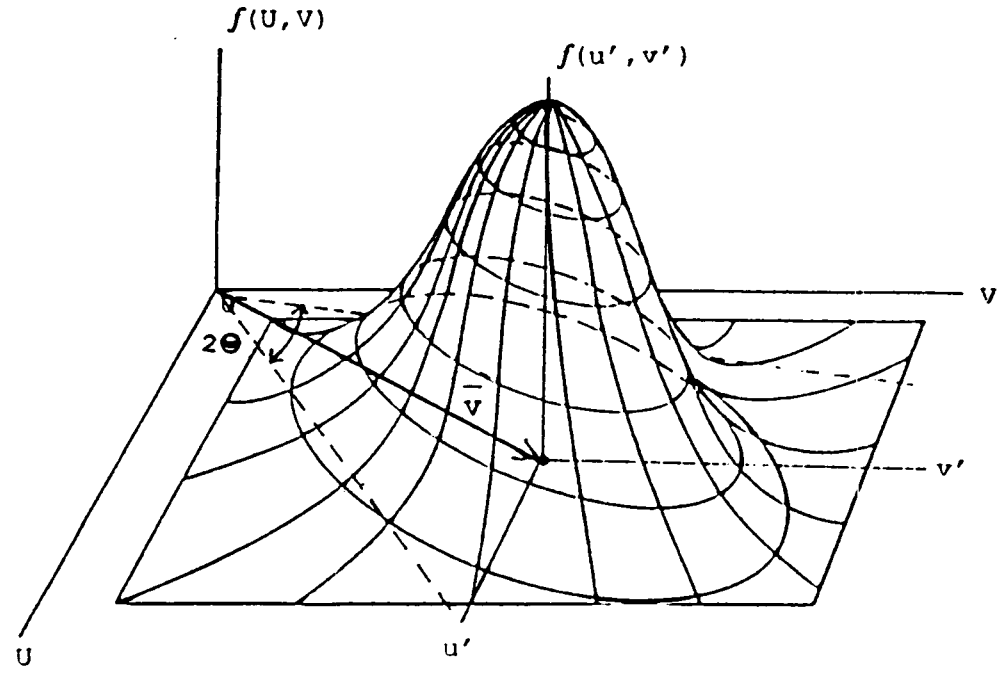

Figure 15 Bivariate normal u,v velocity joint pdf.

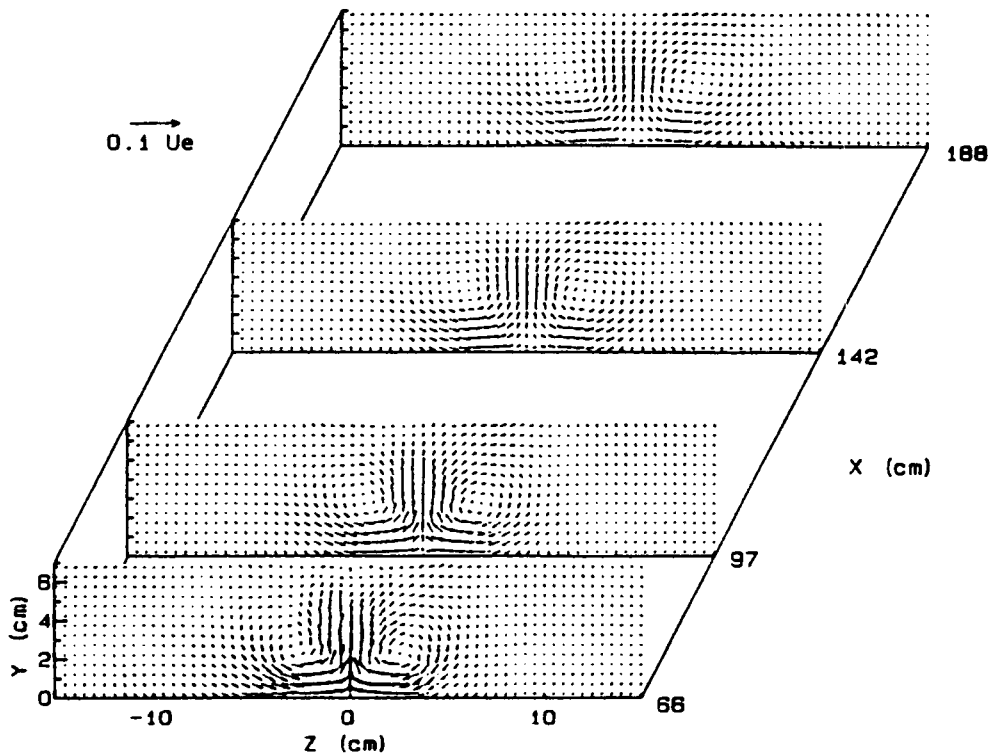

Figure 16 Secondary velocity vectors with cylinder.

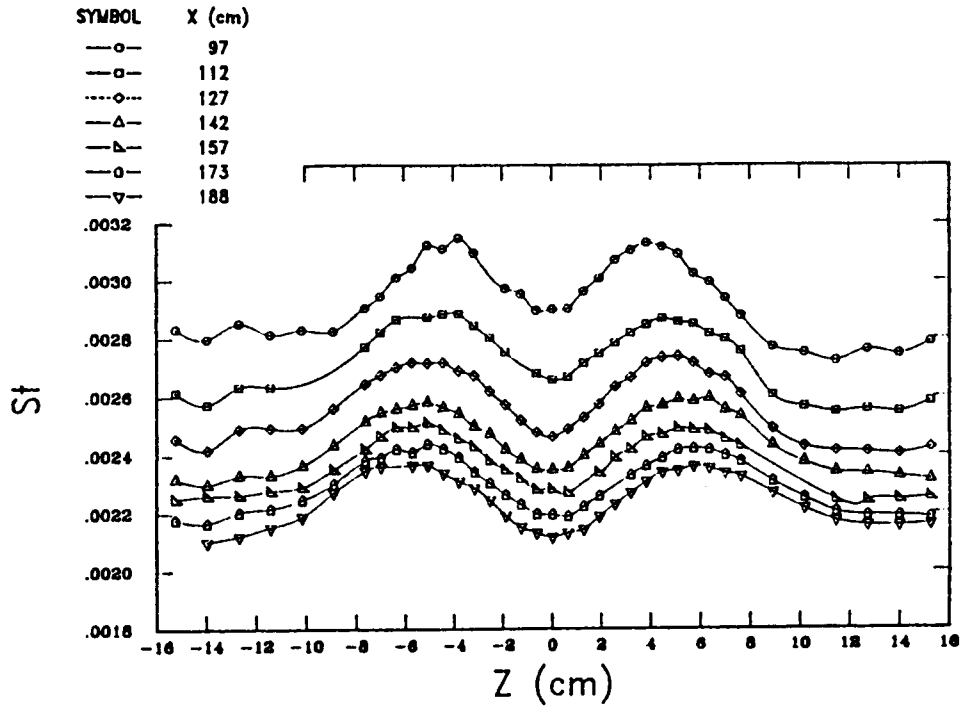

Figure 17 Spanwise distribution of Stanton number with 1 inch cylinder.

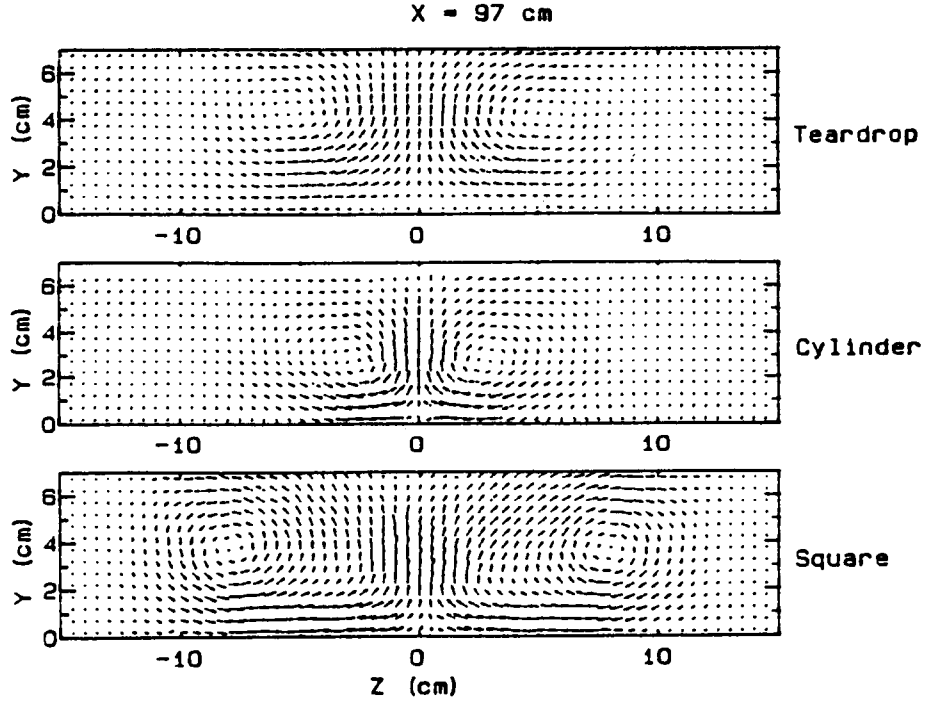

Figure 18 Secondary flow downstream of the three bodies extending from the wall.

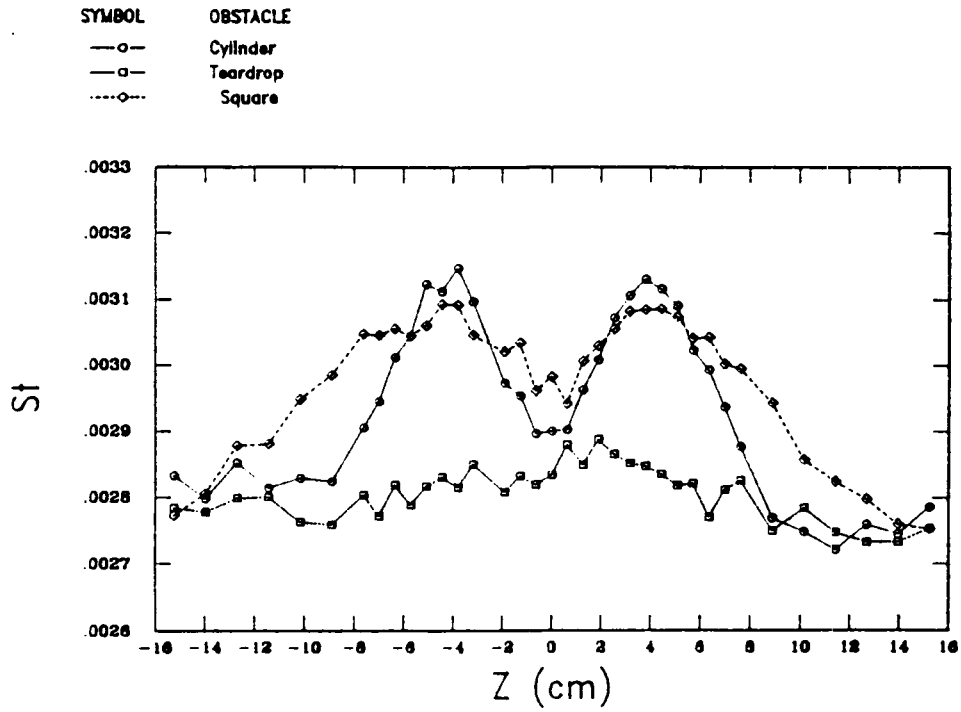

Figure 19 Spanwise distribution of Stanton number: comparison between types of obstacles at X=97 cm.